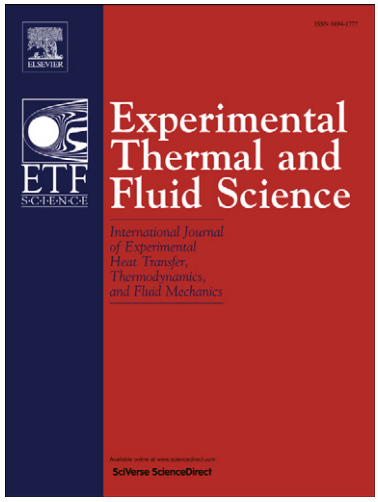

Experimental evaluation of the critical local wall shear stress around cylindrical probes fouled by diesel exhaust gases

Concepción Paz, Eduardo Suárez, Antonio Eirís, Jacobo Porteiro

PII: S0894-1777(11)00247-0
DOI: 10.1016/j.expthermflusci.2011.11.011
Reference: ETF 7611

To appear in: *Experimental Thermal and Fluid Science*

Received Date: 29 July 2011
Accepted Date: 29 November 2011

Please cite this article as: C. Paz, E. Suárez, A. Eirís, J. Porteiro, Experimental evaluation of the critical local wall shear stress around cylindrical probes fouled by diesel exhaust gases, *Experimental Thermal and Fluid Science* (2011), doi: 10.1016/j.expthermflusci.2011.11.011

Experimental evaluation of the critical local wall shear stress around cylindrical probes fouled by diesel exhaust gases

Concepción Paz[a]*, Eduardo Suárez[a], Antonio Eirís[a], Jacobo Porteiro[a]

[a]CFD Simulation Group, University of Vigo, Lagoas Marcosende 9 CP- 36310 Vigo, Spain

*Corresponding author: C. Paz, E-mail:cpaz@uvigo.es, Tel.: +34 986 813 754, Fax: +34 986 812 201

E-mail addresses: suarez@uvigo.es (E. Suárez), eiris@uvigo.es (A. Eirís), porteiro@uvigo.es (J. Porteiro)

Abstract

The problem of fouling in the heat exchangers of exhaust systems has yet to be resolved. This results in enormous costs for engine manufacturers due to the required over-sizing during design and due to unscheduled maintenance needs.

This article presents an experimental layout developed for measuring fouling in diesel engine exhaust gas systems. This facility was based on a circular cylindrical cross-flow device, with one straight and smooth stainless steel probe positioned transverse to the flow of exhaust gases. The probe can be cooled from the inside with water and fouled on the outside as a result of particle deposition from exhaust gases.

The tests were conducted under constant engine operating conditions. Therefore, the asymptotic depth of the fouling layer could be measured at different angular positions at the end of each test.

The critical wall shear stress rate is proposed as the controlling mechanism of the local removal process that leads to different fouling depths around each probe. This is in contrast to the critical velocity concept, which cannot be applied at a local scale due to its formulation. The experimental results, although subject to the usual uncertainties of fouling processes, seem to support this idea.

Keywords: fouling; thickness; particle deposition; critical shear stress; soot.

1. Introduction

In recent years, the requirements imposed on exhaust systems have rapidly increased; turbochargers, intercoolers, catalysts, regenerators, filters, heat exchangers, and a growing number of antipollution

devices are now required. All of these systems suffer from a common problem: they are damaged by fouling, one of the most important design parameters in exhaust gas systems [1].

Fouling is defined as the presence of any foreign substance that is adhered to the heat transfer surface and causes negative effects. It is a complex phenomenon that is influenced by factors such as design, operating conditions, fuel, and oil. The deposition of fouling material on the heat transfer surface decreases thermal transmission [2] and, in most cases, creates an additional layer of material that reduces the flow section and thereby results in pressure losses [3]. Monitoring the evolution of this pressure loss to account for the fouling layer requires expensive control loops and sensors. An understanding of the mechanisms involved in the process and a characterisation of the properties of the accumulated mass are important for the development of effective mitigation techniques.

In this research, a test bench was developed to measure the amount of mass deposited and the local thickness of the fouling layer on devices exposed to diesel exhaust gases. Examination of the deposits adhered to the walls of the probes showed that solid carbon and condensed hydrocarbons were the main constituents of the fouling layer, as observed by other authors [4], and that particle deposition seemed to be the most important mechanism during fouling [5].

In general, the growth of the soot layer can be driven by different physical mechanisms, including sedimentation, interception, diffusion, inertial impaction, electrostatic attraction, thermophoresis and gravitational settling. These mechanisms depend on the nature and size of the particles present and the operating conditions. Fouling is commonly divided into three steps, as proposed by Bott [6]; Epstein expanded this division to include five steps [7]. First, particles are transported from the duct core toward the vicinity of the walls. This transport is related to the particles' relaxation time t_p^+, which characterises the extent to which the drag forces experienced by a particle are affected by fluid velocity changes caused by turbulence. After reaching the proximity of the boundary layer, the particles may travel through this layer because the turbulent effects are substantially decreased and become deposited on the surface. Deposition is a strongly size-dependent process. For $t_p^+ < 0.1$-0.2 (in air, particles diameter below 0.1-0.2µm), the deposition rate is mainly controlled by Brownian diffusion and turbulent dispersion when the temperature gradient is zero. When a temperature gradient exists in the above range, the thermophoretic force becomes important [5]. In the range $0.1 < t_p^+ < 10$, (particle diameter between 1-10µm in air), thermophoretic effect decreases as t_p^+ approaches 10, while turbophoresis and lift force may become

relevant. The impaction regime starts for $t_p^+ >$ 10-20 (about 10-20 μm in air); here, particles are too large to respond to the eddies fluctuations near the wall, therefore, turbophoretic effects becomes less important [8].

Soot particles in diesel exhaust gases are in the range of $10^{-8} \sim 10^{-5} m$, with most typical values on the order of $10^{-8} \sim 10^{-7} m$ [4]. The submicron scale of these particles and the high temperature gradients typical in exhaust systems make thermophoresis the most important deposition effect [9]. When the particles reach the wall at low velocities, chemical and electrostatic forces, such as van der Waals forces, enable sticking or adhesion [10].

In the reverse process, particles are removed and detached from the fouling layer. This process was described by Epstein [11] as dissolution, erosion and spalling. This step, which has likely received the least amount of attention from researchers, involves several mechanisms including turbulent bursts, electrostatic double layer forces [10], and the impacts, rolling and scrubbing actions associated with particles [12, 13]. Removal is considered to be strongly linked to velocity [14]. Finally, the last process is the change of residue properties with time, a process referred to as ageing.

When fouling is dominated by particulate deposition, a stable or asymptotic thickness may be reached [15]. Several researchers, including Messerer et al. [16] and Grillot and Icart [5], have studied the evolution of asymptotic fouling. The most accepted explanation of this phenomenon is that, in confined flows, deposits attenuate heat transfer and increase shear stress. This reduces temperature gradients, which thereby decreases thermophoretic deposition and increases the removal effect, leading to an equilibrium situation [15].

Most previous research has evaluated fouling at a global scale under controlled conditions with plastic or metal particles. In this study, the real working conditions of a diesel exhaust device were reproduced to generate a fouling layer on a cylindrical probe. The local depth of the deposited layer was compared with the local levels of thermophoresis and shear stress, which oppose these forces at a local scale.

2. Experimental set-up

Several reasons justified the experimental setup chosen: the fouled surface can be extracted for its weight and optical inspection, the system generates low backpressure to the engine assuring its stable operation during the test, the shear stress distribution over a cylindrical probe is well documented, it is easy to generated cases with different level of refrigeration, and the geometry generated the range of Reynolds

and t_p^+ we were looking for. In addition, it is easy to simulate numerically which can be useful for the validation of fouling submodels.

The gases used in this fouling study were produced with a CGM10DW generator set composed of a Lombardini LDW 702 and a single pole alternator. In this system, gases were exhausted from a two-cylinder engine working at $3000\,r.p.m.$ submitted to a $6\,kVA$ resistive load. The engine supplied a constant mass flow of approximately $60\,kg/h$ up to approximately $650\,K$. The exhaust gases supplied by the engine arrived through a bifurcation that split the gases between two parallel pipelines, in which two identical automotive EGR coolers were positioned. Before and after each EGR cooler, cylindrical probes were exposed to the gas. The measuring section is shown in Figure 1.

The pressure and temperature measurements were collected with thermocouples and pressures gauges, the locations of which are shown in Figure 1. The positions of the sensors were selected according to the recommendations of each manufacturer. The pressure sensors were of the membrane type and had an accuracy of $\pm 0.05\,mbar$, a relative maximum of $500\,mbar$ and an absolute maximum of $10\,bar$ absolute. The temperature sensors were A class sensors designed for high temperatures (up to $600\,°C$). In the coolant circuit, three wire PT100 temperature sensors were used. When necessary, the check valves at the entrance of the test section could be closed to derive the entire mass flow rate of exhaust gases through a single section of the arrangement ($60\,kg/h$); opening both sides introduced $30\,kg/h$ of exhaust gas into each section.

With this layout, the probes positioned before the heat exchanger (the precooler probes) were subjected to conditions similar to those found at the entrance of EGR coolers, while the probes positioned after the heat exchanger (the postcooler probes) operated under conditions typical of the colder parts of EGR coolers. Due to the weakness of the fouling layer, several attempts to introduce an insertion probe into the heat exchanger to directly measure fouling were unsuccessful.

Finally, the gas under the desired conditions crossed the instrumented section, with the thermocouples and pressures gauges connected to a CPU control system to guarantee stability of the test conditions. Measurements were taken every $100\,s$ and were subsequently stored and averaged. After passing through the control area, the exhaust gases exited the apparatus.

The coolant circuit, shown in Figure 1, was a closed loop of heating-refrigeration equipment controlled by thermocouples, a flowmeter and a control valve that governed the pumping group in the range of 200 to

$3000 l/h$. The coolant fluid was water, and it flowed through the shell side of both heat exchangers. The system maintained the gas temperature in the test section of the postcooler tubes at a constant value.

The cylindrical probe exposed to the cross-flow consisted of a straight AISI 316L tube with an external diameter of $16 mm$ and a thickness of $1 mm$ positioned transverse to the exhaust gas tube, which had an inner diameter of $53 mm$. The blockage ratio, or the cylinder/shell cross-sectional area ratio, was 0.385. The gas flowed around the exterior of the test tube while the coolant flowed through the tubes.

Figure 2 shows fouling around a probe in detail. The tubes could be placed at any angle transverse to the flow direction. To evaluate the effects of gravity on deposition, the horizontal and vertical positions were analysed. The orientations of the tubes relative to the flow direction were marked with a mechanised nick on the incident side of the test tubes to ensure that the reference position of the tube with regard to flow and gravity was not lost.

The overall experimental uncertainty was calculated on the basis of a 95% confidence level, as recommended by Moffat [17]. Using this method, the uncertainties of the measurements were as follows: the fluid temperatures had a tolerance of $\pm 0.35°C$ to $100°C$ and $\pm 0.95°C$ to $400°C$ [18]; the air flow rate was $0.5 \pm 1\%$ of the measured values; the water flow rate was $\pm 1.5\%$ of the measured values; and the fouling thickness was $\pm 1 micron$.

2.1 Experimental procedures

For these studies, all tests were conducted under steady-state conditions. To ensure uniform working conditions, the engine was warmed until all parameters, including the engine temperature and $r.p.m.$, were stabilised. The exhaust gas flows through a bypass circuit in this step. Due to the low efficiency of the probes as heat exchangers, determining the point at which they reached a steady fouling condition was difficult. Assuming an asymptotic evolution of fouling, each test was conducted until all experimental parameters reached a steady level to ensure stabilised conditions. Thus, the end of each test was determined by the efficiency loss of the intermediate heat exchangers in the system.

The experimental program comprised changes in three variables: gas mass flow rate ($30 kg/h$ and $60 kg/h$), coolant temperature ($90°C$, uncooled) and gas temperature, which could vary with the performance of the coolers. Eight different combinations were possible, with a Re number ranging from 7000 to 30000 and a dimensionless particle relaxation time t_p^+ of 0.1 to 1 for the typical exhaust

particle size. Therefore, all tests fell into the subcritical regimen [19], and the influence of the thermophoresis effect was strong [8].

The exact procedure for each test is described below.

- In clean conditions, before starting the test, each probe and each heat exchanger were weighed using an $\pm 0.001 g$ accuracy balance.
- The engine was started and allowed to run until the entire system was warm.
- Exhaust gas started to flow through the experimental section.
- During the test, the temperature, pressure drop and thermal efficiency were monitored.
- Once these parameters reached a steady state, the test was completed.
- The fouled probes and heat exchangers were then carefully removed and weighed.
- The fouling layer of each probe was measured using a profile projector with a 200x magnification lens. Profiles were taken every $5 mm$ in the longitudinal direction and every 45º in the angular position; both end measurements were rejected. Later, all points were numerically smoothed to obtain an average profile.
- At the end of each test, the coolers were cleaned in an ultrasound cleaning bath.

Dismantling the probes was a difficult operation due to the low consistency of the residue and its tendency to crumble. This agrees with the idea that fouling is controlled by particle deposition. Finally, the mass of each probe was scraped and submitted to thermogravimetric analysis, as proposed by Stratakis [20]; that is, the oil and fuel evaporation curves were analysed separately (Table 1). The deposits in the lower mass flow rate cases consisted of roughly twice as much hydrocarbon as those in the higher mass flow cases. Although there is no general consensus on the importance of this substance [21], researchers have claimed that it affects adhesion and the sticking of particles to walls [14].

As mentioned above, the effect of fouling on the thermal efficiency of the probes was imperceptible; therefore, the parameter used to determine the end of each experiment was the thermal efficiency of the coolers. In all cases, the efficiency of the coolers followed the same pattern (Figure 3), and the conventional definition of efficiency [22], Eq.(1), was used:

$$\varepsilon = \frac{T_{g_{in}} - T_{g_{out}}}{T_{g_{in}} - T_{c_{out}}} \quad \textbf{(1)}$$

3. Results

A total of 18 tests were performed (Table 2). No considerable differences between the horizontal and the vertical tubes were observed; hence, gravity effects could be neglected. This is in agreement with other researchers who have noted that gravity is negligible for small particles ($r_p < 5\mu m$) [23].

As mentioned previously, to reduce the uncertainty of the experiments, the profile of the fouling layer was measured longitudinally and averaged. Therefore, one mean value was obtained for each angular position, and an equivalent profile of the fouling layer over each probe was produced. The fouling layer thickness on each probe is shown in Figure 6 and Figure 7. As shown in these figures, the cross-sections of the fouling layers had similar morphologies. In all cases, some common aspects were observed. The flow incidence region is clearly shown in Figure 6 and Figure 7, and the appearance of the fouling matter was somewhat different. The main parameters obtained during the experiments are summarised in Table 2.

The profile of the deposit is shown in Figure 4 and analysed in more detail in Figure 5. In these images, the deposit compositions were compared for three normal planes: I, II, and III, which correspond to incidence with the probe, the lateral side of the probe and the back side of the probe, respectively. Changes in all cases in plane II were apparent, even to the naked eye. These differences were attributed to the action of different deposition mechanisms; thermophoresis was mainly responsible for the smoother look of plane III and the particulate impacts in plane I.

4. Discussion

4.1 Mean values

In this research, two parameters were known to directly affect the overall fouling layer: velocity and temperature gradient. Increases in the mean velocity of gas flow resulted in decreases in the amount of fouling deposition. This relationship was demonstrated by Lepperhoff and Houber [14], and its reduction is associated with the removal effects, as studied by various authors [11, 24]. The link between velocity and fouling has been attributed to the impact of particles on previously deposited particles, to scrubbing action, to the collapse of thick layers, to reentrainment caused by round stressing, to the electrostatic double layer force, and to the turbulent nature of fluid as turbulent bursts.

The temperature gradient effect is closely related to thermal diffusion or thermophoresis. The importance of this deposition mechanism has been exhaustively studied theoretically with models [25], experimentally with latex particles [26], and specifically with soot particles [27]. The authors of these studies have indicated the importance of thermophoresis for small particles.

As shown in our results, increasing the flow velocity from $7.5 m/s$ to $15 m/s$ (approximate values corresponding to $30 kg/h$ and $60 kg/h$, $u = \frac{\dot{m}_g}{\rho A}$) decreased the amount of fouling (Table 2). This reduction was also observed for the fouling thickness profile. All of the test probes showed the same reduction tendency; however, the difference between the precooler position, with a mean reduction of 93.1%, and the postcooler position, with a mean reduction of 8.3%, was significant. This remarkable difference can be explained by the lower temperature gradient in the postcooler cases, which produced a smaller thickness.

The effect associated with the temperature gradient was more obvious. A comparison of equivalent cases with and without the thermal gradient (cooled versus un-cooled probes) for all positions and for any velocity revealed that cooling of the probe resulted in considerable increases in the deposited mass. This effect is clearly shown in the thickness profiles and deposited mass results displayed in Figure 6, Figure 7, and Table 2. This thermophoretic effect produced a mean mass increase of 46.8%.

4.2 Critical flow concept

The *critical flow concept* is one explanation for the relationship between the flow velocity and the amount of fouling suffered by a wall [28]. Under the assumption that rolling is the major removal mechanism, the critical velocity can be calculated. It is defined as the mean flow velocity at which the rolling moment is equal to unity. Velocity values higher than the critical value suggest the rolling of deposited particles and, hence, their movement through the wall.

$$RM = \frac{F_d\left(1.399 - \delta\right)}{\left(F_{adh} + F_g - F_l - F_b\right) d/2} \quad \textbf{(2)}$$

The rolling moment ratio given in Eq.(2) compares the hydrodynamic rolling moment to the adhesion resting moment [29], where F_d is the drag force; δ is the particle deformation; F_{adh}, F_g, F_l and F_b are the adhesion, gravity, lift and buoyancy forces, respectively; and d is the contact diameter.

The critical wall velocity obtained from M. S. Abd-Elhady et al. [30] was compared with results from similar conditions and several surface energy values (Figure 8). As shown in this figure, the critical gas velocity strongly decreased as the particle size decreased, and it was also strongly influenced by the surface energy of the particles. The surface energy appears in the calculation of the adhesion force F_{adh} and in the contact diameter d, according to the expression of Johnson et al. [31], Eq.(3). This equation is a modification of the Hertz contact expressions. Disparities in these values can be found in the literature [32, 33].

$$d^3 = 6r_p\left(\frac{1-v_p^2}{E_p}-\frac{1-v_s^2}{E_s}\right)\left\{L+3\pi\Gamma r_p+\left[3\pi\Gamma r_p L+\left(3\pi\Gamma r_p\right)^2\right]^{1/2}\right\} \quad \textbf{(3)}$$

4.3 Critical wall shear stress

Based on the critical velocity, a new removal parameter is proposed, the critical shear stress τ_w, to establish a local explanation for the fouling profiles of the probes. A simple comparison of the fouling profiles to the shear stress patterns on the probes indicated a possible relation.

Two noticeable regions appear in the flow around smooth circular cylinders: the stagnation point and the separation points. In flows with Reynolds numbers (Re) in the range of 10^3 to $2\cdot10^5$, the separation point is on the top of the cylinder ($90°-100°$ from the stagnation point), and this is reflected by an approximately constant drag coefficient [19]. If the Re is less than approximately $4\cdot10^5$, the boundary layer remains laminar from the stagnation point at the front of the cylinder to the point at which it separates. In both areas, the shear effect of the flow is zero, and the removal effect ceases. Previous experimental results agree with the general appearance of wall shear stress around cylinders or with the skin friction coefficient $\frac{\tau_w}{\frac{1}{2}\rho_\infty u_\infty^2}$ [34]. This indicates a two-lobe structure, with maximum values located at approximately $60°$ on both sides of the stagnation point.

The critical shear stress, which corresponds to the critical flow velocity, is defined as the shear stress at which the rolling moment is equal to unity. Therefore, shear stress values higher than the critical value result in the rolling of deposited particles. For a given particle diameter, the critical wall shear stress τ_{cr}, can be obtained, assuming a constant friction factor *f*, from Eq.(4):

$$u = u_\tau \sqrt{\frac{8}{f}} \tag{4}$$

where u_τ is the friction velocity. Finally, the wall shear stress can be calculated with Eq.(5):

$$\tau_w = u_\tau^2 \cdot \rho \tag{5}$$

Figure 9 shows the wall shear stress rates for the two different flow velocities tested. This figure shows the importance of redefining a local parameter to at least partially explain the final fouled cross-section.

In the areas where the wall shear stress exceeded the critical value for a given particle diameter (i.e., in the figures, ratios larger than 100%), the rolling action should have prevented deposition of the largest particles. Moreover, the rolling of the largest particles probably affected the removal of other sized particles by impacting them; thus, these areas tended to have smaller deposit thicknesses, as shown in Figure 6 and Figure 7. This rate is obviously larger in Figure 9-*a* than in Figure 9-*b* due to the higher velocity. These critical wall shear rate profiles indicate the changing tendency in the size of particles deposited on the separation flow area, and this agrees with the visual results shown in Figure 5.

The importance of using a more local removal parameter (critical shear stress) in place of a mean measure (critical flow velocity) is clear when mean values (Figure 10-*a*) are compared with local parameters (Figure 10-*b*). Based on the mean values, the largest particles barely exceeded the critical condition in the high velocity test. Nevertheless, a considerable portion of the surface was above the rolling condition, even in the low velocity test.

The critical wall shear stresses (Figure 9-*a*) and the fouling thicknesses from two experimental tests (plotted on a magnified scale for clearer comparisons) are superimposed in Figure 11. As shown, the windward (left) half of the tube showed similar behaviour in both cases. The thickness peaks coincided at the stagnation point, where the minimum shear stress was observed. The valleys or minimum fouling

thicknesses were found at approximately ±40° from the stagnation point, where the critical shear stress value was exceeded for the larger particulates.

On the leeward side (right), the difference between the cooled and un-cooled tests was more pronounced. The un-cooled probe was approximately inverse to the lobular critical shear profiles, whereas the cooled probe was apparently unaffected by the local level of shear stress. Moreover, it exhibited more than twice the thickness of the un-cooled probe. Visual inspection (Figure 5) confirmed these changes in the size of the deposited particles.

5. Conclusions

An experimental apparatus was built to investigate the shape and size of the fouling layer deposited by exhaust gases on the surface of cylindrical probes positioned transverse to the flow of the gases. To account for thermophoresis, cooling water was passed through the interior of the probes. This configuration enabled us to collect measurements of the thickness of the fouling layer deposited at different angular positions and the total deposited mass under different operating conditions. A heat exchanger inserted between the two probes enabled the time at which the coolers experienced asymptotic fouling to be assessed at the end of each test.

As expected, increases in the temperature gradient considerably increased the overall thickness of the fouling layer, thus establishing the importance of thermophoresis in the deposition process in diesel exhaust.

The fouling layer profiles at different angular positions, with peaks and valleys, were evaluated. The minimum height occurred at both sides of the stagnation point in all cases.

Reductions in the deposited mass induced by flow velocity increases were also evaluated. This effect has been related to a critical flow velocity that enhances erosion; however, this concept cannot be applied at a local scale. Hence, the critical wall shear stress concept was derived and introduced to quantify local erosion. The analysis and discussion of critical values given here in illustrate the importance of local effects in the deposition of particles. In this study, the shear stress of the clean cylindrical probe was used for simplicity and to avoid simulations of the local shear stresses of the fouled shape. Nevertheless, the fouled cross-section profiles obtained around the cylinders showed a clear connection between erosion and the local shear stress profile.

Tests at different Re numbers and instantaneous measurements of the evolution of the fouling layer will clarify some of the uncertainties identified in this study. However, it can be concluded that the depth of the fouling layer deposited on surfaces exposed to diesel exhaust gases can be related to the local shear stress.

Nomenclature

A	cross-sectional area, (m^2)
d	contact diameter, (m)
D_h	hydraulic diameter, (m)
E	Young's modulus, (Pa)
f	friction factor, $f = \frac{2\tau_w}{\rho u^2}$, dimensionless
F_d	drag force, (N)
F_{adh}	adhesion force, (N)
F_g	gravity force, (N)
F_l	lift force, (N)
F_b	buoyancy force, (N)
L	load, (N)
$\dot{m}$	mass flow rate, (kg/s)
r_p	particle radius, (m)
Re	Reynolds number, $\mathrm{Re} = \frac{\rho u D_h}{\mu}$, dimensionless
RM	rolling moment ratio, dimensionless
T	temperature, (K)
t_p^+	particle relaxation time, $t_p^+ = \frac{2\rho_p r_p^2 \rho_g u_\tau^2}{9\mu}$, dimensionless
u	velocity, (m/s)
u_τ	friction velocity, (m/s)
v	Poisson's ratio, $v = -\frac{d\tau_{transverse}}{d\tau_{axial}}$, dimensionless

Greek symbols

δ	particle deformation, (m)
ε	thermal efficiency, dimensionless
Γ	surface energy, (J/m^2)
μ	dynamic viscosity, (Pa s)
ρ	density, (kg/m^3)
τ_w	wall shear stress, (Pa)

Subscripts and superscripts

c	coolant
g	gas
in	inlet
out	outlet
p	particle
s	surface
∞	free-stream (far away from the walls)
*	critical

Acknowledgements

The authors are grateful to BorgWarner Turbo and Emissions Systems for financial support of this research.

Bibliography

[1] H. Teng, G. Regner, Characteristics of Soot Deposits in EGR Coolers, Society of Automotive Engineering, 01-2671 (2009).
[2] T.R. Bott, L.F. Melo, Fouling of heat exchangers, Experimental Thermal and Fluid Science, 14(4) (1997) 315-315.
[3] J.E. Hesselgreaves, The efect of system parameters on the fouling performance of heat exchangers, Proceedings of the 3rd UK National Conferenceon Heat Transfer and1st European Conference on Thermal Sciences, Institute of Chemical Engineering, (1992).
[4] D.B. Kittelson, Engines and nanoparticles: a review, Journal of Aerosol Science, 29(5-6) (1998) 575 - 588.
[5] J.M. Grillot, G. Icart, Fouling of a cylindrical probe and a finned tube bundle in a diesel exhaust environment, Experimental Thermal and Fluid Science, 14(4) (1997) 442 - 454.
[6] T.R. Bott, Gas side Fouling, Fouling Science and Technology, (1988) 191-206.
[7] N. Epstein, General thermal fouling models, Fouling Science and Technology, Proceedings of the NATO Advanced Study Institute, (1988) 15-30.
[8] A. Guha, Transport and Deposition of Particles in Turbulent and Laminar Flow, Annual Review of Fluid Mechanics, 40 (2008) 311-341.

[9] M. Albarham, J. Hoard, D. Assanis, D. Styles, E.W. Cortis, N. Ramesh, C.S. Sluder, J.M.E. Storey, Modeling of Thermophoretic Soot Deposition and Hydrocarbon Condensation in EGR Coolers, Society of Automotive Engineering, 01-1939 (2009).
[10] R. Oliveira, Understanding adhesion: A means for preventing fouling, Experimental Thermal and Fluid Science, 14(4) (1997) 316-322.
[11] N. Epstein, Fouling: Technical aspects, Fouling of heat transfer equipment, (1981) 31-53.
[12] N.-H. Kim, R.L. Webb, Particulate fouling of water in tubes having a two-dimensional roughness geometry, International Journal of Heat and Mass Transfer, 34(11) (1991) 2727 - 2738.
[13] D. Bouris, E. Konstantinidis, S. Balabani, D. Castiglia, G. Bergeles, Design of a novel, intensified heat exchanger for reduced fouling rates, International Journal of Heat and Mass Transfer, 48(18) (2005) 3817 - 3832.
[14] G. Lepperhoff, M. Houben, Mechanisms of deposit formation in IC engines and heat exchangers, Society of Automotive Engineering, 931032 (1993).
[15] A. Stolz, K. Fleischer, W. Knecht, J. Nies, R. Strähle, Development of EGR coolers for truck and passenger car aplication, Society of Automotive Engineers, 2001-01-1748 (2001).
[16] A. Messerer, R. Niessner, U.Poschl, Thermophoretic deposition of soot aerosol particles under experimental conditions relevant for modern diesel engine exhaust gas systems, Journal of Aerosol Science, 34 (2003) 1009-1021.
[17] R.J. Moffat, Describing the uncertainties in experimental results, Experimental Thermal and Fluid Science, 1 (1988) 3-17.
[18] DIN/IEC 751 Reference platinum precision resistance thermometers, in, International Electrotechnical Commission, 1983.
[19] B.M. Sumer, J. Fredsoe, Hydrodynamics around cylindrical structures, World Scientific, 1997.
[20] G.A. Stratakis, A.M. Stamatelos, Thermogravimetric analysis of soot emitted by a modern diesel engine run on catalyst-doped fuel, Combustion and Flame, 132(1-2) (2003) 157 - 169.
[21] C.S. Sluder, J.M.E. Storey, S.A. Lewis, D. Styles, J. Giuliano, J. Hoard, Hydrocarbons and Particulate Matter in EGR Cooler deposits: Effects of gas flow rate, coolant temperature, and oxidation catalyst, Society of Automotive Engineering, 01-2467 (2008).
[22] F.P. Incropera, D.P. Dewit, Fundamentals of heat and mass transfer, Wiley, 1996.
[23] M.M. Sharma, H. Chamoun, D.S.H.S.R. Sarma, R.S. Schechter, Factors controlling the hydrodynamic detachment of particles from surfaces, Journal of Colloid and Interface Science, 149(1) (1992) 121 - 134.
[24] M. Bohnet, Fouling of heat transfer surfaces, Chemical Engineering Technology, 10 (1987) 113-125.
[25] S.A. Gokoglu, D.E. Rosner, Thermophoretically augmented mass transfer rates to solid walls across laminar boundary layers, The American Institute of Aeronautics and Astronautics Journal, 24 (1986) 172-179.
[26] C.-J. Tsai, J.-S. Lin, S.G. Aggarwal, D.-R. Chen, Thermophoretic deposition of particles in laminar and turbulent tube flows, Aerosol Science and Technology, 38:2 (2004) 131-139.
[27] A.D. Eisner, D.E. Rosner, Experimental studies of soot particle thermophoresis in nonisothermal combustion gases using thermocouple response techniques, Combustion and Flame, 61(2) (1985) 153 - 166.
[28] N. Epstein, Elements of particle deposition onto nonporous solid surfaces parallel to suspension flows, Experimental Thermal and Fluid Science, 14(4) (1997) 323 - 334.
[29] F. Zhang, A. Busnaina, M. Fury, S.-Q. Wang, The removal of deformed submicron particles from silicon wafers by spin rinse and megasonics, Journal of Electronic Materials, 29 (2000) 199-204.
[30] M.S. Abd-Elhady, T. Zornek, M.R. Malayeri, S. Balestrino, P.G. Szymkowicz, H. Müller-Steinhagen, Influence of gas velocity on particulate fouling of exhaust gas recirculation coolers, International Journal of Heat and Mass Transfer, 54(4) (2011) 838 - 846.
[31] K.L. Johnson, K. Kendall, A.D. Roberts, Surface Energy and the Contact of Elastic Solids, Proc. R. Soc. London, (1971) 301.
[32] K. Kendall, Solid surface energy measured electrically, Journal of Physics D: Applied Physics, 23 (1990) 1329.
[33] E. Papirer, S. Li, H. Balard, J. Jagiello, Surface energy and adsorption energy distribution measurements on some carbon blacks, Carbon, 29 (1991) 1135 - 1143.
[34] D.W. Ballengee, C.F. Chen, Experimental determination of the separation point of flow around a circular cylinder, Dowdell, R.B. (Ed.), Flow; its Measurement and Control in Science and Industry, (1971) 419-427.

List of figures

List of tables

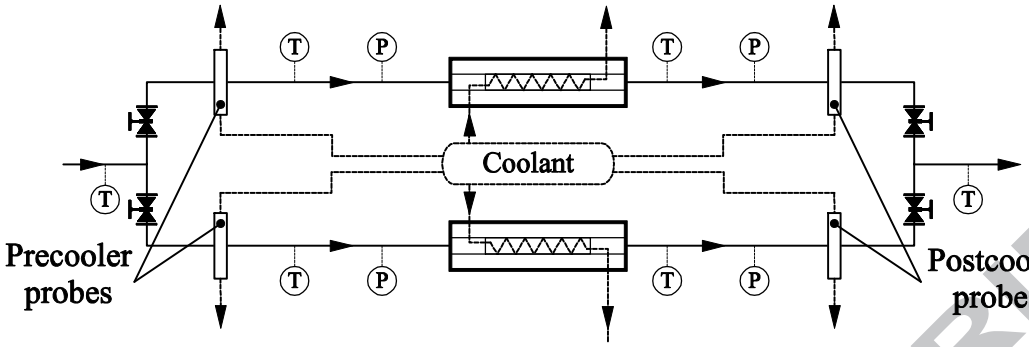

Fig.1: Scheme of measuring section

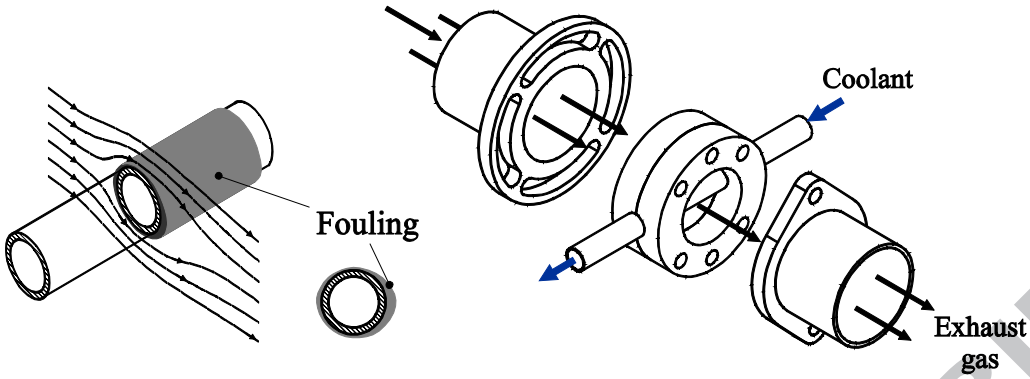

Fig.2: Scheme of fouled tube assembly

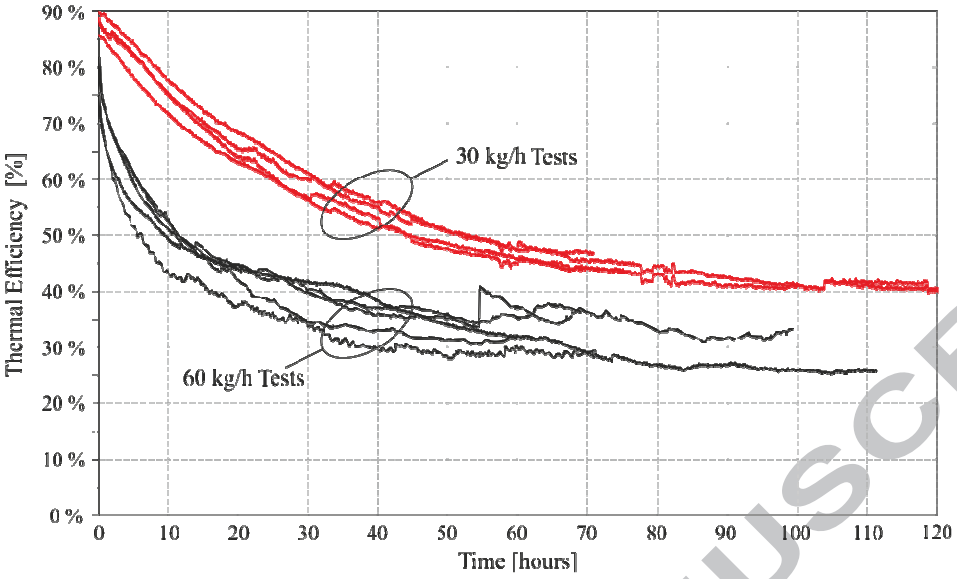

Fig.3: Thermal efficiency evolution

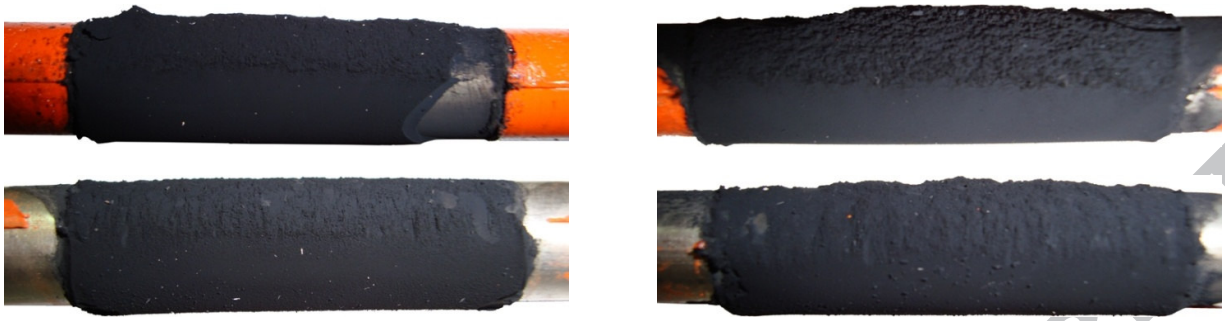

Fig.4: Photographs of fouling layer outside 4 of the 18 tested tubes

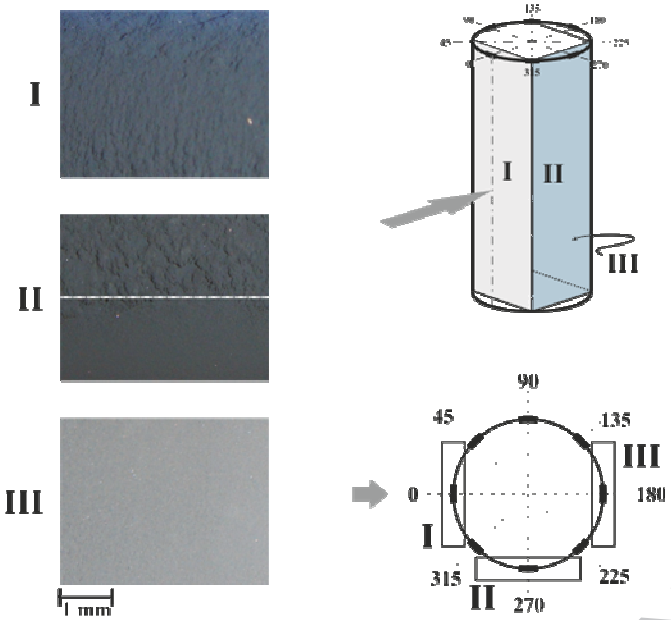

Fig.5: Aspect of fouling deposited on the test tubes

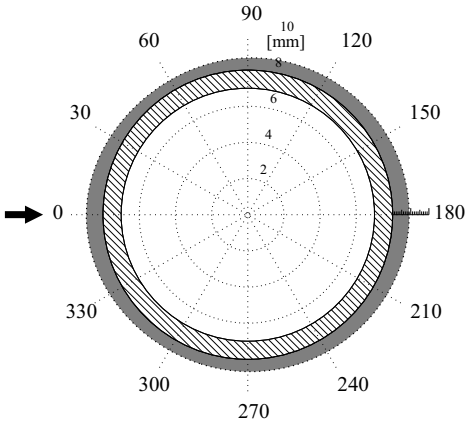

$60\,kg/h$ Precooler position

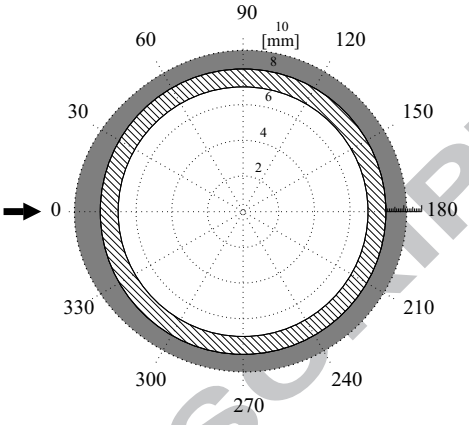

$30\,kg/h$ Precooler position

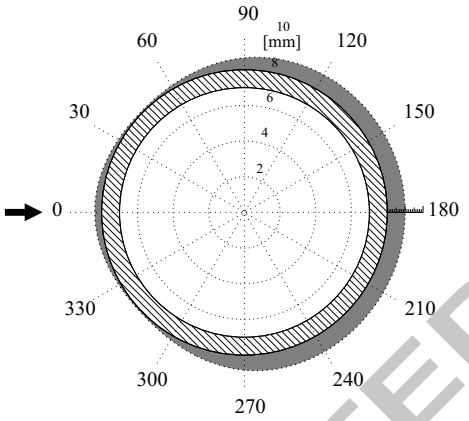

$60\,kg/h$ Postcooler position

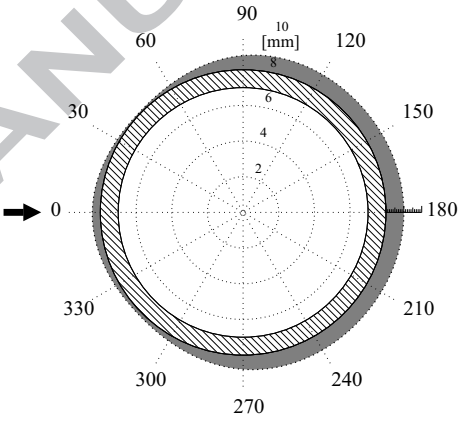

$30\,kg/h$ Postcooler position

(a) Thickness resulting from $60\,kg/h$ gas mass flow.

(b) Thickness resulting from $30\,kg/h$ gas mass flow.

Fig.6: Fouling thickness of the probes with internal refrigeration

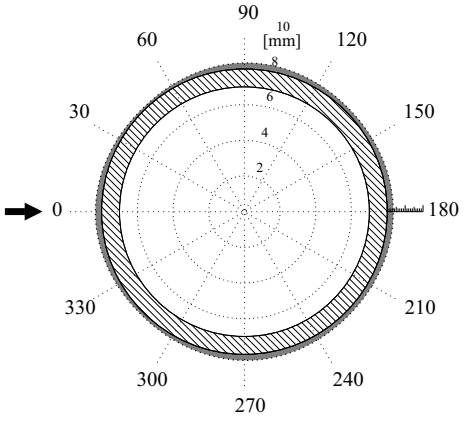

$60\,kg/h$ Precooler position

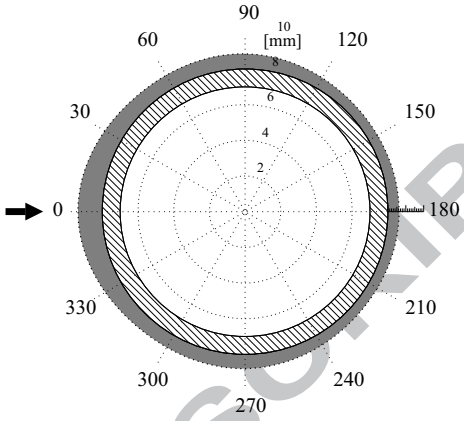

$30\,kg/h$ Precooler position

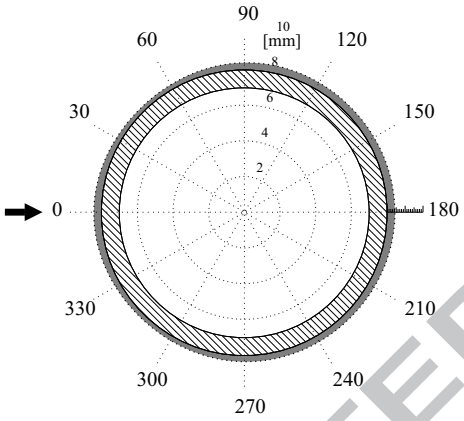

$60\,kg/h$ Postcooler position

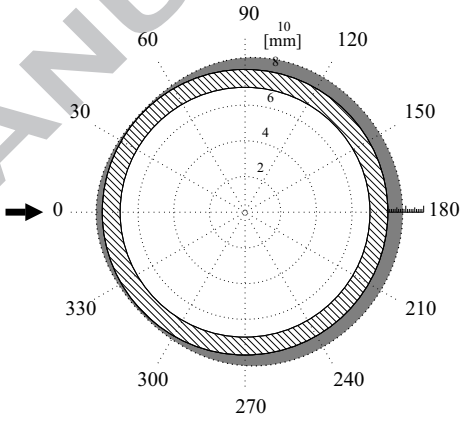

$30\,kg/h$ Postcooler position

(a) Thickness resulting from $60\,kg/h$ gas mass flow.

(b) Thickness resulting from $30\,kg/h$ gas mass flow.

Fig.7: Fouling thickness of the probes without internal refrigeration

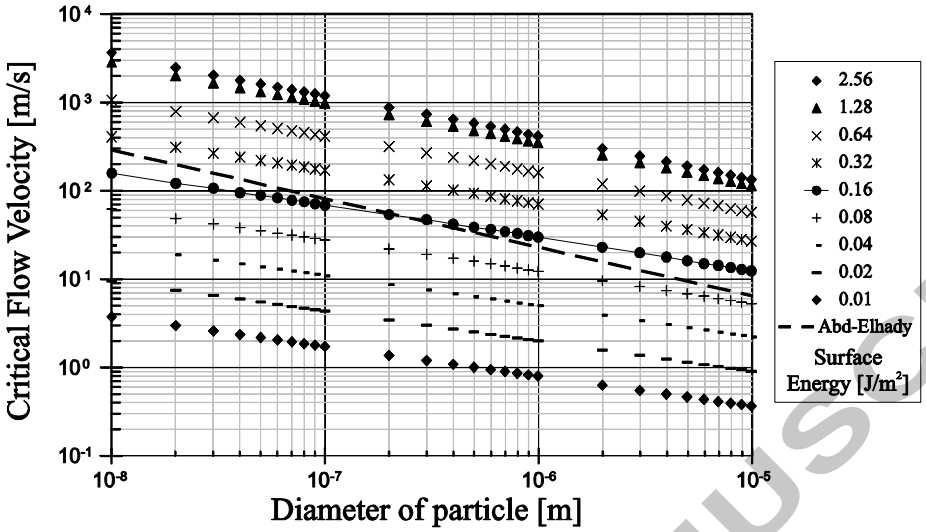

Fig.8: Critical flow velocity and influence of energy surface values

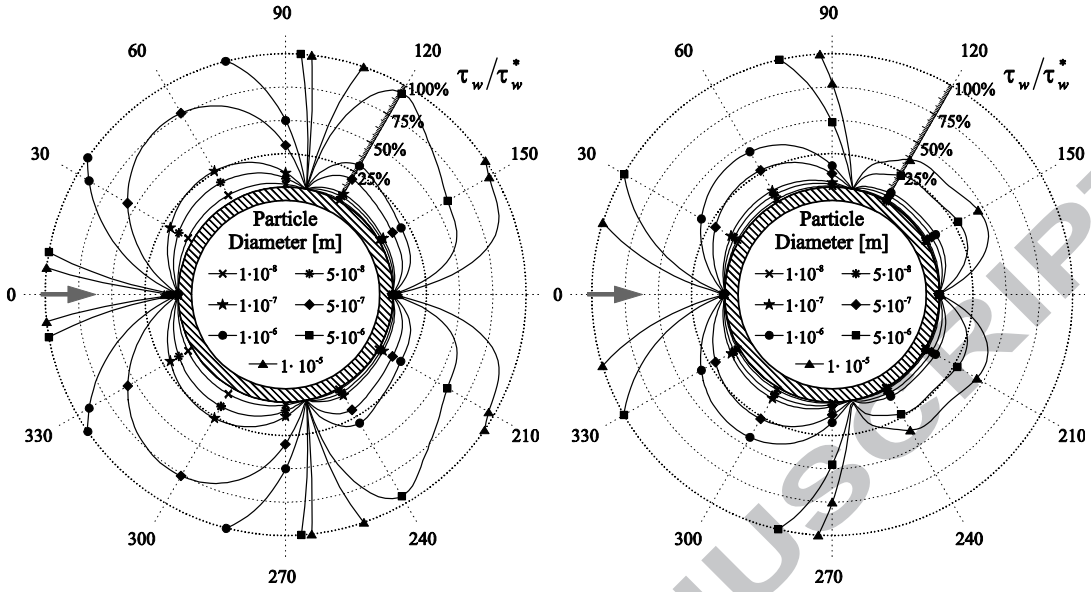

(*a*) 60 *kg / h* (*b*) 30 *kg / h*

Fig.9: Critical wall shear stress rate

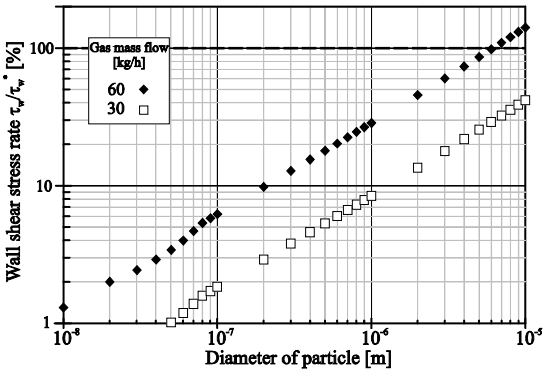

(a) Wall shear stress mean rate.

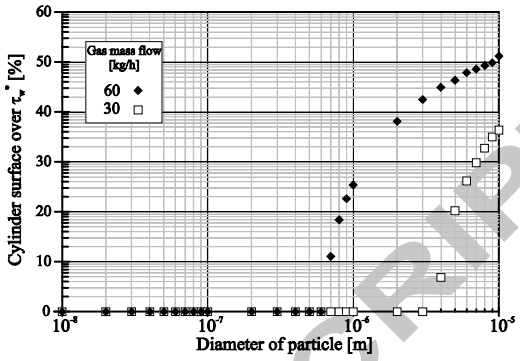

(b) Cylinder surface over.

Fig.10: Mean versus local measurement of critical parameters

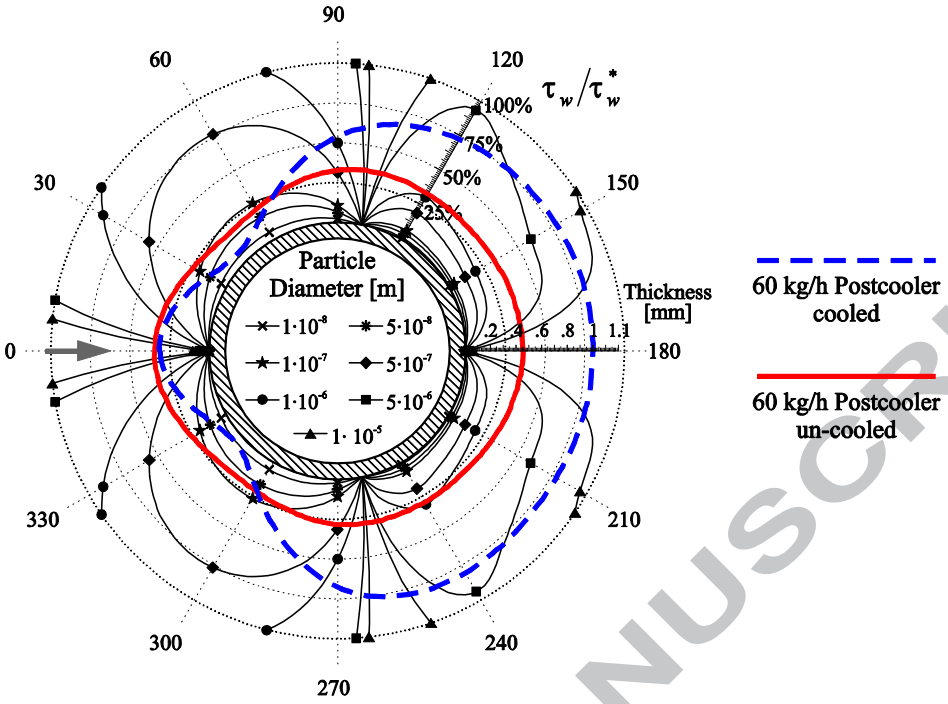

Fig.11: Fouling thickness results superimposed on critical shear stress values.

Table 1: Hydrocarbon content of deposited residue (results of TG-DSC analysis).

	$60\,kg/h$ tests				$30\,kg/h$ tests			
Sample	1	2	3	4	5	6	7	8
Hydrocarbon %	11.2	14.2	12.2	14.5	25.9	23.8	24.5	33.8

Table 2: Mass deposited by tube for 30 and $60\,kg/h$ gas mass flows.

	Test Nº		Experimental mass (mg)		Inlet gas temperature (ºC)	
Mass Flow (kg/h)	60	30	60	30	60	30
Precooler cooled	1, 5, 11	9, 15	45.72	32.98	380	380
Postcooler cooled	4, 6, 13	8, 18	27.42	26.93	154-293*	125-264*
Precooler un-cooled	3, 14	7, 17	27.49	11.10	380	380
Postcooler un-cooled	2, 12	10, 16	17.27	15.05	154-293*	125-264*

*Temperature varied during test.

Highlights

Experimental apparatus to investigate fouling layer deposited by diesel exhaust gases

Cylindrical probes transverse to the flow of gas until asymptotic fouling

Measurements of the evolution of the fouling layer at angular positions

Critical wall shear stress concept was derived to quantify local erosion.

Depth of the deposit can be related to the local shear stress

Graphical abstract

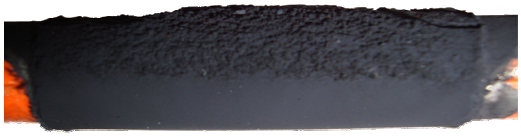

FOULING